J. metamorphic Geol., 2001, **19,** 699–715

High-grade metamorphism and hydrous melting of metapelites in the Pinos terrane (W Cuba): Evidence for crustal thickening and extension in the northern Caribbean collisional belt

A. GARCÍA-CASCO,[1] R. L. TORRES-ROLDÁN,[1] G. MILLÁN,[2] P. MONIÉ[3] AND F. HAISSEN[4]
[1]*Departamento de Mineralogía y Petrología, Universidad de Granada, Fuentenueva s/n, 18002-Granada, Spain, (agcasco@ugr.es)*
[2]*Instituto de Geología y Paleontología, Via Blanca y Carretera Central, La Habana, Cuba*
[3]*Laboratoire de Tectonique et Géochronologie, URA CNRS 1371, USTL, Place E. Bataillon, 34095 Montpellier Cédex, France*
[4]*Département de Géologie, Faculté des Sciences, Université Chouaib Doukkali, B.P. 20, El Jadida, Morocco*

ABSTRACT The Pinos terrane (Isle of Pines, W Cuba) is a coherent metamorphic complex that probably represents a portion of the continental margin of the Yucatan Block during the Mesozoic. Within the framework of other metamorphic terranes in the Greater Antilles, the Pinos terrane is characterized by the occurrence of high-grade kyanite-, sillimanite- and andalusite-bearing metapelites and migmatites. Assessment and modelling of phase relations in these high grade rocks indicate that they reached a peak temperature of *c.* 750 °C at 11–12 kbar, and then underwent strong decompression to *c.* 3 kbar at *c.* 600 °C. Decompression was contemporaneous with the main synmetamorphic deformation in the area (D2), and was accompanied by segregation of trondhjemitic partial melts formed by wet melting of metapelites. Metamorphism terminated in the Uppermost Cretaceous (68 ± 2 Ma; $^{40}Ar/^{39}Ar$ dates on biotite and muscovite). The *P–T–t*-deformation relations of the high-grade rocks suggest that crustal thickening (during collision of this portion of the Yucatan margin with the Great Volcanic Arc of the Caribbean?) was followed by decompression interpreted to reflect exhumation by extension, possibly related to the initial development of the Yucatan Basin in the uppermost Cretaceous.

Key words: Caribbean; crustal thickening; pelite melting; Pinos Island; tectonic extension.

INTRODUCTION

The metamorphic basement of the Isle of Pines, herein called the Pinos terrane, is one of the so-called South-western Cuban terranes that also include the Guaniguanico and Escambray terranes (Fig. 1b). All these terranes have a continental foundation and are made of comparable Jurassic to Upper Cretaceous terrigenous and carbonatic sequences (up to the Eocene in Guaniguanico terrane), that formed on the southern margins of the North American Plate and Yucatan block (e.g. Millán, 1997a; Iturralde-Vinent, 1996, 1997; Marton & Buffler, 1999; Pszczólkowski, 1987, 1999; Cobiella-Reguera, 2000). These margins were involved in the Late Cretaceous to Eocene build up of the Cuban Orogenic Belt as a consequence of their collision with the Great Arc of the Caribbean (Fig. 1a; Burke, 1988; Pindell & Barrett, 1990; Draper & Barros, 1994; Iturralde-Vinent, 1996, 1997; Gordon *et al.*, 1997; Mann, 1999).

The metamorphic histories of the various South-western Cuban terranes are distinct. The Guaniguanico terrane underwent high-*P*, low-grade metamorphism along the Cangre sliver, adjacent to the Pinar de Río Fault (Somin & Millán, 1981; Pszczólkowski & Albear, 1985; Millán, 1988). In the Escambray terrane most tectonic slices also underwent high-*P* metamorphism, with development of blueschist and eclogite facies assemblages (Somin & Millán, 1981; Millán & Somin, 1981; Millán, 1997c). The prevalence of high-*P* metamorphism in the Guaniguanico and Escambray terranes suggests subduction/accretion of the Yucatan margin beneath the Cretaceous Great Arc of the Caribbean plate (Millán, 1997a), analogous to other Caribbean metamorphic complexes that represent fragments of the North American passive margin (e.g. the Asunción terrane of eastern Cuba, the Samaná peninsula of northern Hispaniola, Millán & Somin, 1985; Lewis & Draper, 1990; Joyce, 1991; Goncalves *et al.*, 2000). In the Pinos terrane, however, metamorphism reached high-grade conditions (Somin & Millán, 1981; Millán, 1981, 1997b; Babushkin *et al.*, 1990), suggesting that this part of the ancient Caribbean plate boundary had a different tectonic setting. The current contribution, a study of high-grade rocks in the Pinos terrane, is aimed at providing additional constraints on the metamorphic evolution of this terrane and a consideration of the implications with regard to

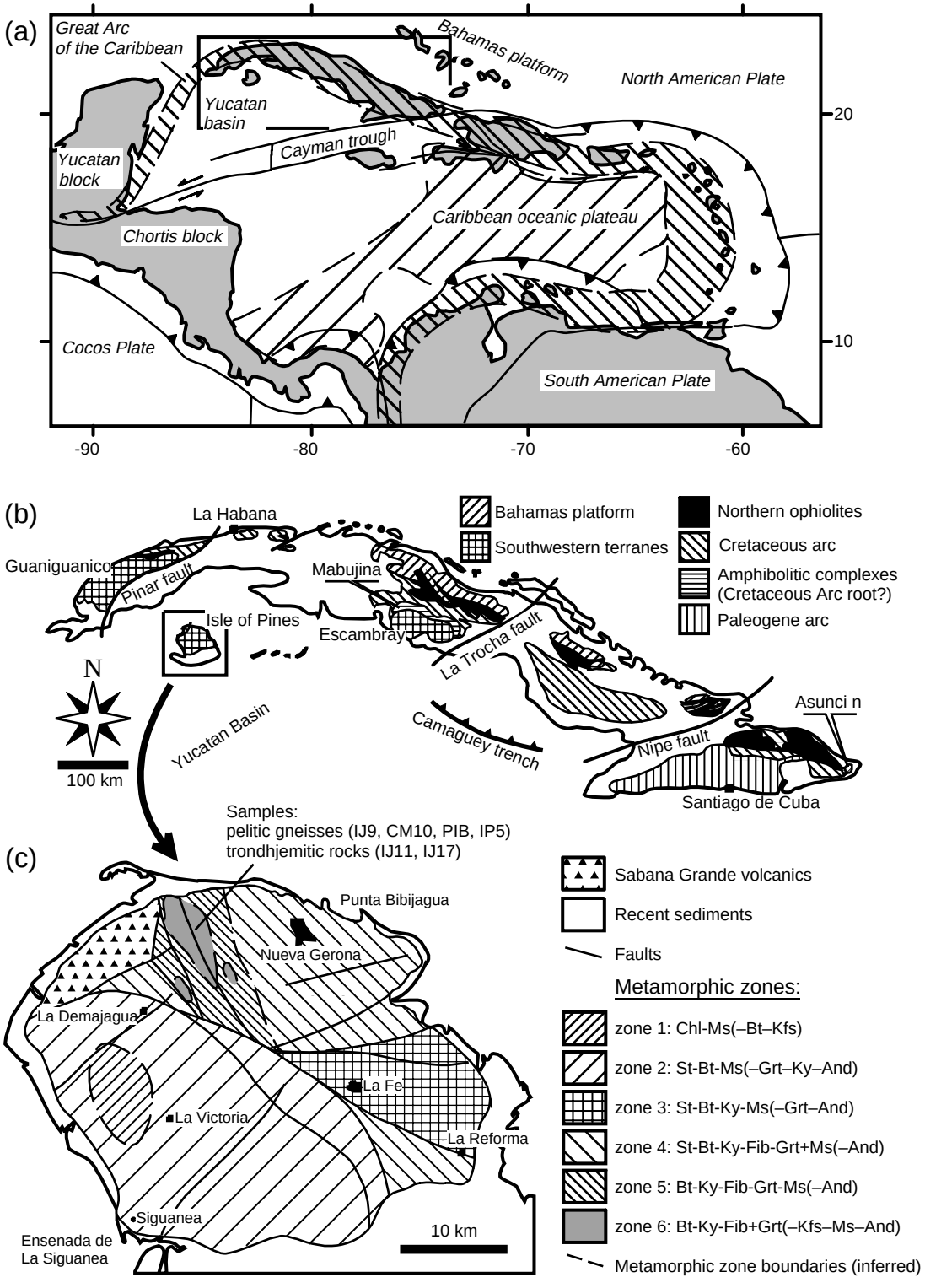

Fig. 1. (a) Plate tectonic configuration of the Caribbean region, with indication of important geological features (after Draper *et al.*, 1994; Mann, 1999). (b) Geological sketch map of Cuba showing location of the south-western metamorphic terranes (after Iturralde-Vinent, 1996). (c) Metamorphic map of the Isle of Pines (slightly modified after Millán, 1997b).

tectonic development of the northern margin of the Caribbean plate.

GEOLOGICAL AND PETROLOGICAL SETTING

The main geological features of the Isle of Pines have been described by Millán (1981, 1997b), Somin & Millán (1981), Pardo & Moya (1988), Pardo (1990), and Babushkin *et al.* (1990). The Pinos metamorphic terrane occupies most of the crystalline core of the island (Fig. 1c), except to the NW where it is overlain by the Sabana Grande volcanic rocks, representing a tectonic fragment of the Cretaceous Volcanic Arc. The metamorphic core consists of terrigenous and carbonate metasediments with occasional metabasite intercalations, that can be correlated with the Jurassic sequences of the Guaniguanico terrane of western Cuba (San Cayetano and Jagua Formations of the Sierra de los Organos). Four main phases of deformation have been identified. The main phase D2 transposes early D1 structures (S1, recorded within garnet and staurolite porphyroblasts), and develops tight folds (F2), the main foliation (S2) and a stretching NW-trending lineation (L2), all of which are syn-metamorphic. The deformation phase D3 is late-metamorphic, characterized by crenulation of S2 (S3), while deformation phase D4 is late- to post-metamorphic, characterized by large-scale open folds and near-vertical faults. Available K–Ar radiometric data from metamorphic rocks scatter from 78 ± 4 to 49.3 ± 3.8 Ma (see Iturralde-Vinent *et al.*, 1996; for review). Late- to post-metamorphic felsic subvolcanic rocks have K–Ar ages of 68–60 Ma (Buguelski *et al.*, 1985).

Metamorphism spans low to high grade conditions (Fig. 1c). In medium grade metapelites garnet, staurolite, and kyanite form pre-D2 porphyroblasts, sillimanite defines the main foliation S2, and andalusite formed after D2. Except for the lack of staurolite, similar relations appear in the high grade metapelites. Late post-D3 secondary micas and chlorite in the schists, amphibole, epidote and chlorite in amphibolites, and the formation of carbonate and sulphide (pyrite $\pm$ pyrrothite) veins, attest for widespread lower temperature retrogression and fluid infiltration. Metamorphism in the Pinos terrane has been interpreted by Millán (1981, 1997b) to represent a unique Upper Cretaceous event, characterized by prograde kyanite-sillimanite (Barrovian type) that is overprinted by retrograde post-D2 andalusite, although Babushkin *et al.* (1990) consider prograde metamorphism to be of Lower Cretaceous age and andalusite overgrowth to be a distinct metamorphic event of Upper Cretaceous age. Regional metamorphism was followed by 'tectonomagmatic reactivation' at 68–60 Ma (Pardo, 1990), that included regional doming and fracturing, emplacement of subvolcanic dykes, hydrothermal and metasomatic alteration, and formation of ores.

SAMPLES AND METHODS

High-grade rocks are restricted to the NW sector of the island (Fig. 1c, metamorphic zone 6) and consist predominantly of well foliated pelitic gneisses that contain less severely deformed mm- to m-sized leucocratic pods, layers and veins of trondhjemitic (s.l.) composition with microgranitic to pegmatitic textures. Intense weathering and soil development precludes direct surface sampling of fresh material. Samples were taken from core wells from metamorphic zone 6 provided by the Empresa Geólogo-Minera Isla de la Juventud, although their precise location within that zone is unknown. Four samples of pelitic gneiss (IJ9, CM10, IP5, and PIB) and two leucocratic pods (IJ11 and IJ17) with none, or negligible evidence of low-T alteration were selected for detailed textural and mineral composition study.

All elemental analyses were done at the University of Granada. Whole-rock major-element determinations were carried out by XRF on glass beads. Precision was better than $\pm 1.5\%$ for an analyte concentration of 10 wt.%. Zr was determined by XRF on pressed powder pellets, with a precision better than $\pm 4\%$ at 100 p.p.m. concentration. Other trace-elements were analyzed by ICP-MS with precisions better than $\pm 2\%$ and $\pm 5\%$ for concentrations of 50 and 5 p.p.m., respectively. Mineral compositions and electronic images were obtained using a CAMECA SX-50 microprobe under operating conditions similar to those described by García-Casco *et al.* (1993).

Phase diagrams were generated using CSpace software of Torres-Roldán *et al.* (2000). For the P–T calculations, we used the TWQ software (v. 2.02) of Berman (1991), that takes advantage of the standard thermodynamic data and mixing models of Berman (1988), Berman (1991), Fuhrman & Lindsley (1988; for plagioclase) and Chatterjee & Froese (1975; for muscovite). Mineral and end-member abbreviations are after Kretz (1983), except Al-silicate polymorphs (Als), fibrolitic sillimanite (Fib), H_2O-fluid (V), and silicate melt (L).

BULK CHEMISTRY, MINERAL ASSEMBLAGES AND FABRICS

The samples of pelitic gneiss have bulk compositions typical of ordinary pelites in terms of major elements (with $K_2O > Na_2O$ and relatively low CaO) and REE patterns (Taylor & McLennan, 1985; Table 1), and are chemically similar to the medium-grade staurolite-bearing metapelites in the same terrane (Fig. 2). They are formed of Grt + Bt + Fib + Pl + Qtz + Rt + Ilm, plus graphite. Kyanite is present in samples IJ9, PIB and CM10, and pyrrhotite is present in samples IJ9 and PIB. Fibrolite and biotite define the main foliation (S2, Fig. 3a, h). Garnet forms pre-D2 poikiloblasts that occasionally preserve a relict foliation (S1) defined by inclusion trails of quartz, biotite, rutile and graphite (Fig. 3b). Garnet is ubiquitously replaced by syn- to post-D2 fibrolite and biotite ($\pm$Pl$\pm$Qtz$\pm$Ilm; Fig. 3a, b, c, d). Kyanite, that also forms pre-D2 porphyroblasts, is directly replaced by syn-D2 fibrolite/sillimanite and post D2 andalusite (Fig. 3e, f), and may include small garnet corroded by the host kyanite (Fig. 3a, g). One significant feature that is common to all samples of pelitic gneiss is the presence of millimetre sized patches or layers rich in quartz and plagioclase, with scarce internal deformation and sharp to diffuse boundaries that generally follow the main foliation S2 (Fig. 3h). These leucocratic zones contain no K-feldspar, but they typically host undeformed idiomorphic (post-D2) muscovite which is lacking in the surrounding darker pelitic material. Replacement of the undeformed muscovite laths by post-D2 biotite, plagioclase and andalusite (Fig. 3i) is the only reaction texture observed within the trondhjemitic layers, which is particularly common when they happen to be adjacent to corroded garnet along the diffuse boundaries with the host pelitic material.

The leucocratic samples IJ11 and IJ17 are trondhjemitic rocks (Fig. 2b) that resemble the leucocratic patches in the pelitic gneisses in that they contain muscovite and are essentially undeformed, indicating crystallization after the major ductile deformation event

of the area (D2). Sample IJ11 is a medium grained, igneous-looking rock formed of Qtz + Pl + Ms + Bt, with minor K-feldspar, apatite and zircon. Plagioclase and quartz form crystals of up to 3 mm in length. Biotite occurs as medium grained crystals dispersed in the matrix and included within porphyritic plagioclase, in all cases with inclusions of zircon and metamict haloes. Muscovite appears as medium grained idiomorphic crystals dispersed in the matrix, often associated with matrix biotite in composite Ms-Bt clots where muscovite overgrows biotite. Finer-grained muscovite (plus Al-silicate, probably andalusite) also replaces plagioclase along preferred crystallographic directions. K-feldspar (< 5% vol), appears as fine xenomorphic interstitial crystals that are interpreted to have crystallized late. Sample IJ17 is a coarser-grained, pegmatite-looking rock consisting of Qtz + Pl + Ms, with minor K-feldspar plus albite replacing muscovite (Fig. 3j).

Table 1. Chemical composition of pelitic gneisses (CM10, IJ9P), a diffuse zone rich in Qtz + Pl within pelitic gneiss IJ9 (IJ9G), and trondhjemite (IJ11). See text for analytical methods and precision estimates.

Sample	CM10	IJ9P	IJ9G	IJ11
Major elements (wt percentage):				
SiO_2	61.73	74.99	76.63	74.17
TiO_2	1.15	0.75	0.56	0.30
Al_2O_3	19.30	9.23	11.54	15.77
Fe_2O_3	8.88	7.73	5.92	1.53
MnO	0.14	0.14	0.11	0.02
MgO	2.39	1.90	1.17	0.24
CaO	0.93	1.03	1.08	1.36
Na_2O	0.83	0.83	1.70	4.26
K_2O	2.57	2.01	1.65	1.80
P_2O_5	0.18	0.09	0.12	0.12
L.O.I	2.21	1.72	0.92	0.89
Total	100.30	100.41	101.39	100.46
Trace elements (p.p.m.)				
Zr	273	392	319	128
Rb		101	54.7	94.0
Be		1.63	2.48	6.88
Sr		100	172	192
Ba		266	183	316
Y		22.9	20.2	5.49
Pb		13.9	23.5	44.4
U		1.86	1.38	7.24
Th		8.40	6.72	21.30
La		26.5	20.1	33.0
Ce		56.1	43.8	69.2
Pr		6.63	5.31	7.86
Nd		24.8	20.2	27.3
Sm		5.02	4.09	4.91
Eu		1.01	1.27	1.07
Gd		4.52	3.81	2.92
Tb		0.70	0.62	0.32
Dy		3.94	3.68	1.28
Ho		0.90	0.76	0.18
Er		3.01	2.43	0.44
Tm		0.49	0.47	0.06
Yb		3.47	3.10	0.37
Lu		0.59	0.54	0.05

Evaluation of the relationship between the pelitic gneisses and the larger decimetre to metre sized leucocratic pods of trondhjemite is hampered in the field because of intense weathering. At the scale of the well-core samples (centimetre to millimetre), however, the scarce internal deformation of the diffuse trondhjemitic patches and layers, their intimate mingling with the pelitic material, and their common arrangement parallel to S2 (including oriented trails of syn-S2 fibrolite, Fig. 3h), are strong indications that most or all the leucocratic material in the higher grade zone of the Pinos terrane formed after local, syn-D2 segregation from the pelitic gneisses (i.e. was not injected from an external source). Additional evidence for local segregation is given by the fact that the vectors joining the compositions of two portions of sample IJ9 (IJ9P richer in pelitic material, IJ9G richer in leucocratic material) trend in the direction of trondhjemite IJ11 (Fig. 2a, b). The segregations could have formed either through partial melting or metamorphic differentiation (Ashworth, 1985). However, the REE pattern of trondhjemite sample IJ11 lacks an Eu anomaly and is richer in LREE and distinctively poorer in HREE than the pelitic gneiss IJ9P (Fig. 2c), which argues in favour of partial melting inasmuch as subsolidus differentiation is known to produce REE-poor patterns and a strong positive Eu anomaly (Sawyer & Barnes, 1988; Whitney & Irving, 1994). The lack of an Eu anomaly in trondhjemite IJ11, which points to a significant participation of plagioclase in the reactions that formed the segregation, is particularly consistent with the expectations for wet (i.e. H_2O-vapour present) melting of plagioclase-bearing metapelites (e.g. Ashworth, 1985; Whitney & Irving, 1994; Patiño Douce & Harris, 1998).

MINERAL CHEMISTRY

Garnet

In the pelitic gneisses, all types of garnet (porphyroblasts and inclusions within kyanite, Fig. 4) have

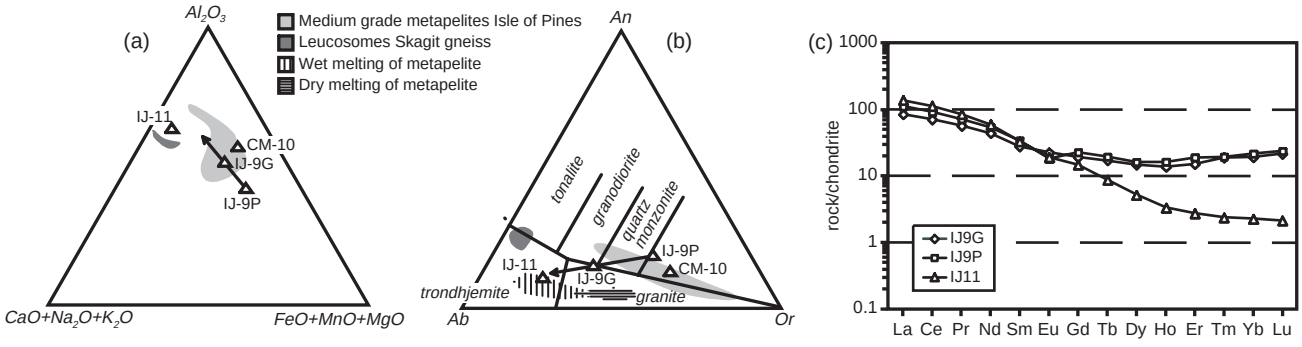

Fig. 2. Whole-rock composition of high grade pelitic gneisses (IJ9P, CM-10), diffuse zones rich in Qtz + Pl within the pelitic gneisses (IJ9G), and trondhjemitic pods (IJ11) from the Pinos terrane in terms of (a) wt percentage of oxides (b) mole percentage of feldspar end-members, with indication of the fields of felsic igneous rocks (O'Connor, 1965; Barker, 1979), and (c) chondrite-normalized REE patterns (chondrite composition after McDonough & Sun, 1995). In (a) and (b), the fields for medium grade metapelites of the Isle of Pines (unpublished data), the trondhjemitic leucosomes from the Skagit gneiss (Whitney & Irving, 1994) and the experimental liquids formed after wet and dry melting of pelites (Patiño Douce & Harris, 1998) are shown for comparison.

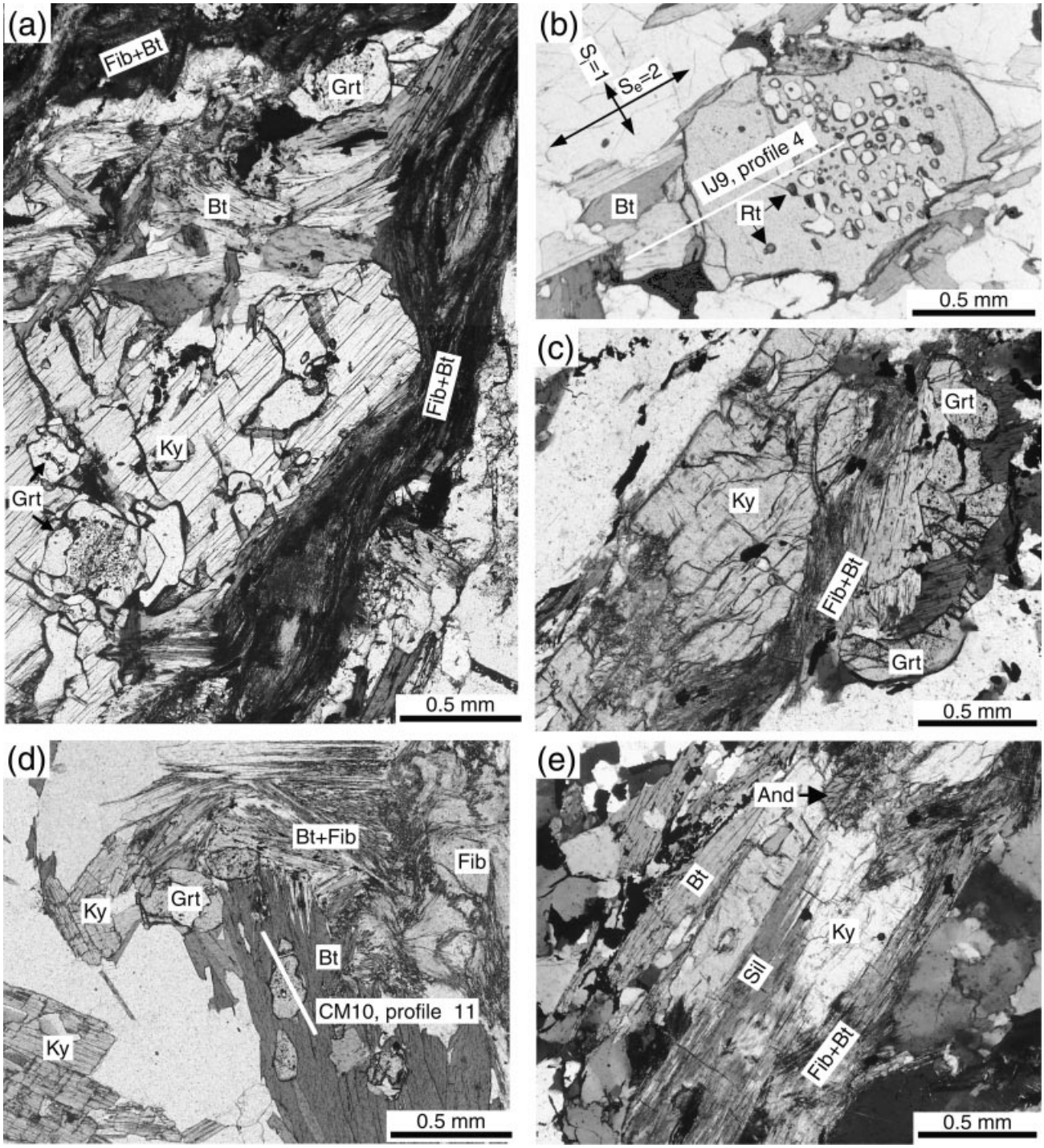

Fig. 3. Representative textures in the pelitic gneisses and trondhjemitic segregates. (a) Pre-S2 kyanite porphyroblasts with corroded garnet inclusions and fibrolite + biotite defining the main foliation S2. (b) Pre-S2 garnet porphyroblast partially replaced by biotite that follows the main foliation S2. Inclusions of quartz and rutile define an older foliation (S1). (c) and (d) Pre-S2 kyanite and garnet partially replaced by biotite and fibrolite. (e) Kyanite partially replaced by sillimanite and andalusite, with biotite and fibrolite defining the main foliation S2. (f) Post-D2 andalusite replacing pre-D2 kyanite porphyroblast. (g) BSE image showing pre-D2 garnet inclusions within kyanite (garnets are corroded by host kyanite). (h) Trondhjemitic segregates within pelitic gneiss parallel to S2 defined by fibrolite + biotite. (i) BSE image of post-D2 replacements of Bt + And + Pl after muscovite and garnet. Note the absence of Kfs in the replacements. (j) BSE image of replacements of muscovite by Kfs + Ab in post-D2 trondhjemitic pegmatite IJ17. Note the absence of Al-silicate. In (b), (d), and (g), the lines mark the location of composition profiles shown in Fig. 4.

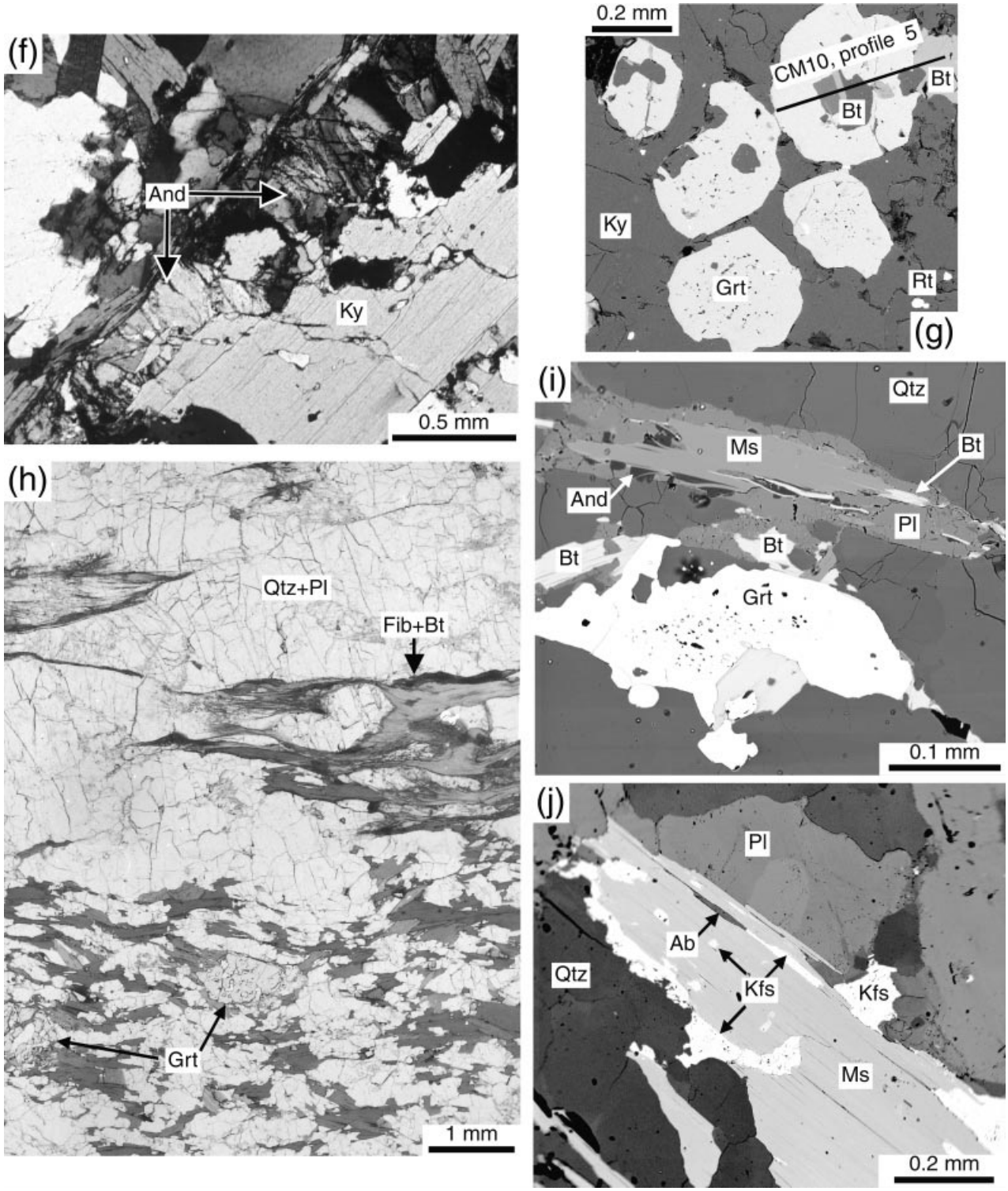

Fig. 3. Continued.

homogeneous cores and narrow retrograde rims where Mg# ($=Mg/(Mg+Fe^{2+}$) decreases and Mn increases, as is typical of high-grade garnet affected by volume diffusion at peak temperature (i.e. peak garnet) and dissolution during retrogression (e.g. Tracy, 1982; Spear, 1991). The compositional relations of corroded garnet and the presence of all three Al-silicate polymorphs in the replacements suggest

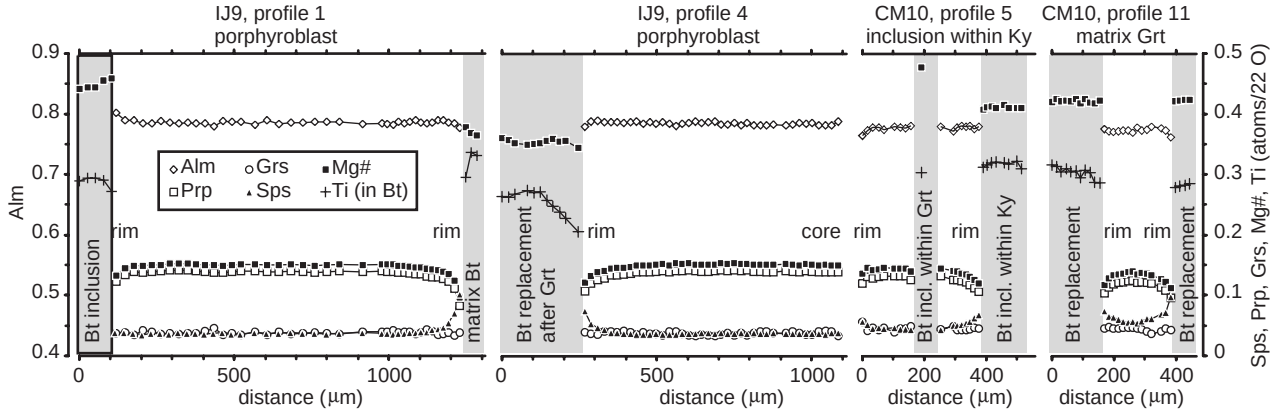

Fig. 4. Representative zoning profiles in garnet and adjacent biotite (inclusions and replacements; see Fig. 3 for location of the profiles).

that retrogression was triggered at high pressure, within the kyanite stability field, and progressed though the sillimanite and andalusite stability fields (cf. Brown & Earle, 1983).

Biotite

Matrix and replacement biotite also resemble those commonly found in high grade metapelites (cf. Guidotti, 1984) and are characterized by high, though variable, Ti contents (up to 0.4 apfu; Fig. 5). Mg# values are remarkably constant, however, and allow no clear chemical distinction between matrix grains and those in the syn- to post-D2 Bt + Als replacements after garnet. The same trend is apparent within single zoned biotite grains that replace garnet, where Ti decreases and Fe and Mg increase toward the Bt–Grt interface but Mg# is constant (Fig. 4, IJ9 profile 4). These observations suggest that matrix biotite does not retain its pre-D2 composition that was in equilibrium with the garnet cores (cf. Spear & Parrish, 1996, Kohn & Spear, 2000), as is also suggested by the fact that the composition of syn- to post-D2 matrix/replacement biotite in the pelitic gneisses is similar to that of post-D2 biotite from trondhjemite IJ11 (Fig. 5).

The pre-D2 inclusions of biotite within garnet have intermediate Ti (0.2–0.3 apfu) and distinctively higher Mg# (up to 0.5, Fig. 5) than syn- to post-D2 grains. Towards the interface of these biotite-garnet pairs, however, Mg# in biotite and garnet increase and decrease, respectively, while Mn in garnet is constant (Fig. 4, IJ9 profile 1). This conforms to the expectations for an Fe-Mg exchange couple isolated from the matrix during retrogression, and hence it is likely that neither these biotite grains retain their original Mg# in equilibrium with peak garnet (cf. Spear & Parrish, 1996).

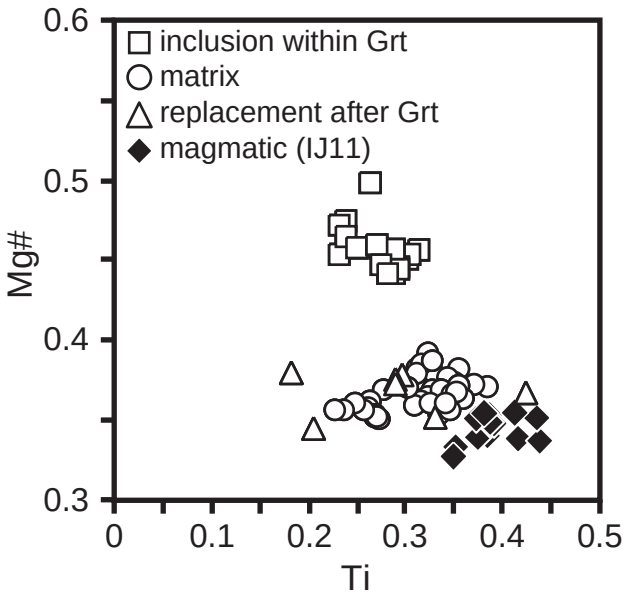

Fig. 5. Composition of biotite from the pelitic gneisses and the trondhjemitic rocks in terms of Ti and Mg# contents.

Plagioclase

In the pelitic gneisses, plagioclase porphyroblasts are unzoned or show slight concentric reverse zoning (Fig. 6) characterized by homogeneous cores and Ca-richer rims (X_{an} = up to 0.25), the latter being similar to matrix grains (X_{an} = 0.22–0.27). The Na-richer homogeneous cores have the highest K contents, and hence could represent equilibrium conditions at peak temperature (cf. Seck, 1971). On the other hand, the composition of plagioclase from the replacements after muscovite and garnet is richer in Ca (X_{an} up to 0.32), which suggests that increasing Ca contents developed as garnet decomposed during retrogression.

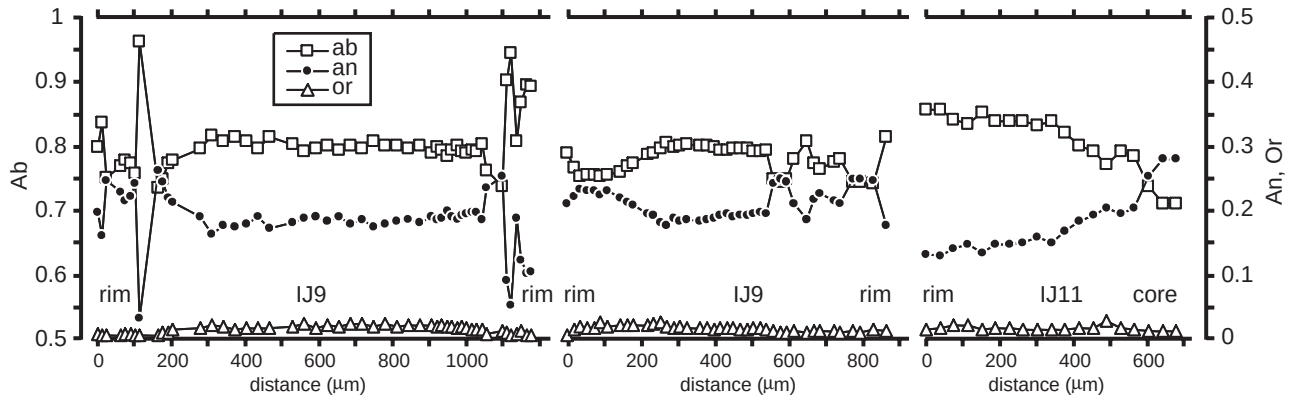

Fig. 6. Representative zoning profiles of plagioclase from pelitic gneiss IJ9 and trondhjemite IJ11.

A latest compositional readjustment is represented by patches of low-K albite (X_{an} down to 0.03) that locally overprint the concentric zoning of plagioclase porphyroblasts (Fig. 6).

Plagioclase in the trondhjemitic samples IJ11 and IJ17 is more albitic than those of the pelitic gneisses. In IJ11, the crystals show normal zoning ($X_{an} = 0.28$–0.12; Fig. 6), and matrix grains are compositionally similar to the phenocrysts rims ($X_{an} = 0.12$–0.15). In IJ17, plagioclase phenocrysts are unzoned ($X_{an} = 0.09$–0.13), but plagioclase that replaces muscovite is nearly pure albite ($X_{an} = 0.05$). Thus, the trends of plagioclase composition in the trondhjemitic rocks contrast with those from the pelitic gneisses (i.e. normal vs. inverse). These differences provide additional support for an anatectic origin of the trondhjemites, in that plagioclase composition in the pelitic gneisses was controlled by garnet dissolution, whereas magmatic crystallization in the trondhjemitic segregates controlled plagioclase composition in these rocks.

Muscovite

Undeformed muscovite from the leucocratic patches in the pelitic samples and trondhjemite IJ11 have low Si (< 6.2 apfu) and high Ti (up to 0.17; Fig. 7) contents, typical of high grade and magmatic muscovite (Miller *et al.*, 1981; Guidotti, 1984). In trondhjemite IJ11, low Ti contents (0.03–0.05 atoms) characterize the rims of the crystals, indicating subsolidus reequilibriation at relatively low temperature. The pegmatite-sized muscovite from sample IJ17 has homogeneous low Ti contents (Fig. 7), which likely derives from the TiO_2-subsaturated nature of this sample. No reaction zoning is apparent in relation with the Kfs + Ab replacements.

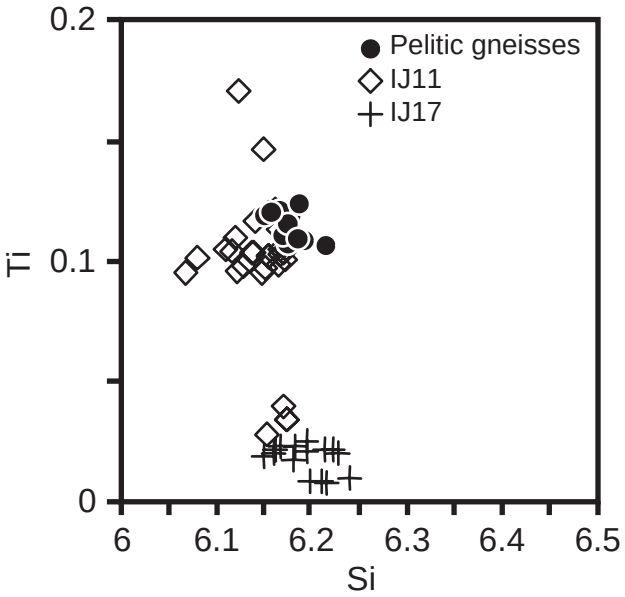

Fig. 7. Composition of muscovite from the leucocratic pods within the pelitic gneisses (IJ9, PIB) and the trondhjemitic rocks (IJ11 and IJ17).

P–T–t PATH

Peak *P–T* conditions

A precise estimate of peak-*T* conditions using the garnet-biotite Fe-Mg exchange thermometer is not possible given that Mg# of all kinds of biotite in the pelitic gneisses (matrix and inclusions) were readjusted during retrogression, including the high-Ti matrix grains located far from garnet. Upon retrogression, however, the isolated biotite-garnet pairs of the garnet interiors evolved through the Fe-Mg exchange reaction:

$$\mathrm{Alm} + \mathrm{Phl} = \mathrm{Prp} + \mathrm{Ann}, \qquad (1)$$

while matrix/replacement biotite and the dissolved rims of garnet evolved both through exchange (1) and net transfer reactions (see below for the nature of these reactions). This implies that in each case the former peak composition of biotite was driven towards higher and lower Mg#, respectively (Fig. 8a, see Spear & Florence, 1992), hence that the composition of 'peak'

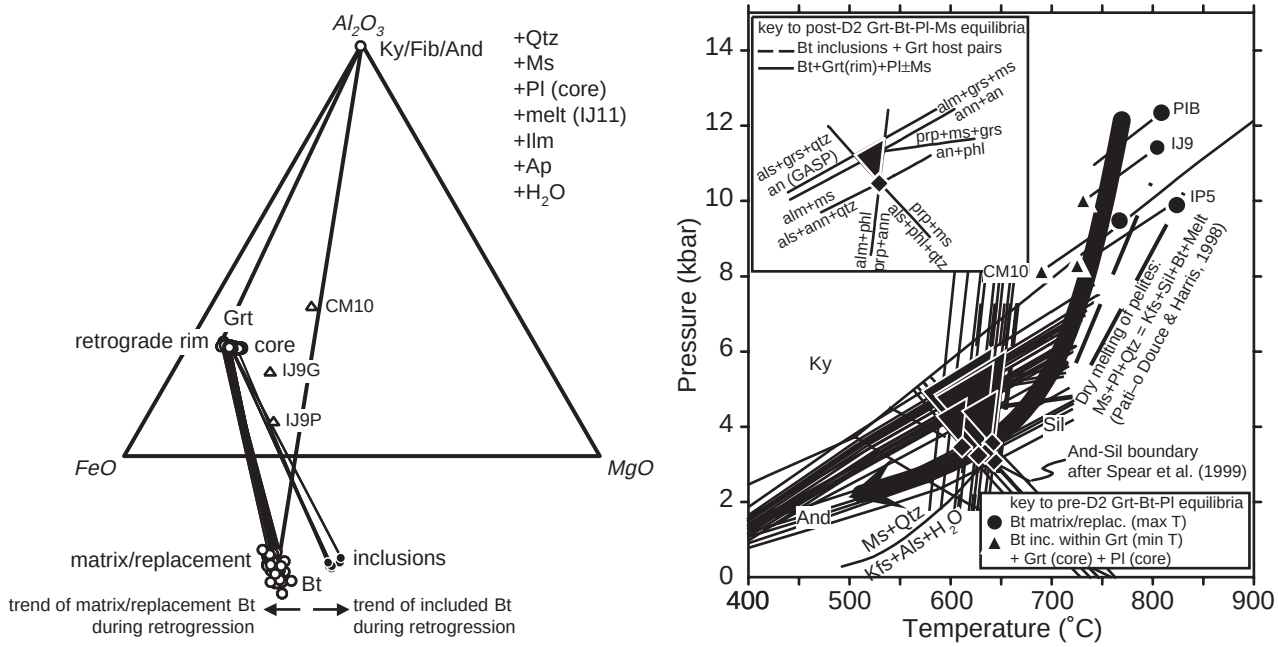

Fig. 8. (a) Phase relationships for pelitic gneiss IJ9 in the AFM diagram after projection from Qtz + Ms + Pl + Ilm + Ap + H_2O + Melt (with the composition of sample IJ11). The tie-lines for the Grt-Bt-Als (matrix) and Grt-Bt (inclusion) assemblages correspond to triplets and pairs of adjacent grains. (b) *P–T* estimates for peak and retrogression conditions of pelitic gneisses IJ9, CM10, IP5 and PIB (see text for further details).

biotite must have had an Mg# comprised between that of biotite inclusions with the minimum Mg# and that of biotite in the matrix/replacements with maximum Mg#. In combination with the unmodified cores of garnet, these compositions allow the calculation of minimum and maximum temperatures that bracket peak-*T*, respectively.

The corresponding temperature bracket so calculated is in the range 700–800 °C for a total calculated range of pressures of 8–12 kbar (Fig. 8b), the latter based on the grossular-Al-silicate-quartz-anorthite (GASP) barometer using the same compositions of garnet cores and the homogeneous cores of plagioclase porphyroblasts. We are less confident in the pressure estimates resulting from samples IP5 (which does not contain kyanite) and CM10 (which has Ca-rich plagioclase with little compositional variation), so our preferred pressure estimate, extracted from samples IJ9 and PIB is 11–12 kbar.

Conditions during retrogression

Simultaneous solutions of the garnet-biotite thermometer and the GASP barometer using lowest-Mg# retrograde garnet rim compositions and adjacent biotite (from inclusions and replacements), plus Ca-rich plagioclase from grains produced after garnet and plagioclase porphyroblasts rims, yield 575–650 °C and 4–6 kbar (Fig. 8b). However, Ca across the retrograde garnet rims is approximately constant, regardless of the extent of retrogression, which suggests that the Ca content in retrogressed garnet rims may not be fully equilibrated with plagioclase. This incomplete equilibration may reflect slow diffusion of Ca^{2+} in garnet during retrogression (Chakraborty & Ganguly, 1991; Schwandt *et al*., 1996), in which case the GASP pressure values should be viewed as maximum estimates. In fact, the equilibrium:

$$\mathrm{Alm} + \mathrm{Ms} = \mathrm{Als} + \mathrm{Ann} + \mathrm{Qtz}, \qquad (2)$$

that is not affected by these problems, yields consistently lower pressures of *c.* 3 kbar at 600–650 °C (Fig. 8b) using the composition of the phases involved in the post-D2 Bt + And + Pl replacements after Ms + Grt. Although these conditions conflict with the predicted stability of andalusite (present in the replacements) as calculated with TWQ, we judge them a better estimate for latest retrogression since they agree with the thermal stability of andalusite as proposed by Pattison (1992) and Spear *et al*. (1999).

P–T–t relations

The calculated *P–T* conditions point to a significant decompression ($\Delta P = -8$ to 9 kbar) at relatively high temperature, suggesting fast exhumation of the terrane during the main deformation (D2) of the rocks. The time of final exhumation of the Pinos terrane was Uppermost Cretaceous, as indicated by the 68 ± 2 Ma clustering of $^{40}Ar/^{39}Ar$ plateau ages of biotite, muscovite and amphibole from high grade samples IJ9 and IJ11, and other medium grade samples from the

Pinos terrane (unpublished data). The overlap of the $^{40}Ar/^{39}Ar$ cooling ages of metamorphic minerals, and of these and the whole-rock K–Ar ages of post-metamorphic subvolcanic dykes (68–60 Ma, Buguelski *et al.*, 1985), additionally points towards high rates of cooling along the low pressure sections of the exhumation *P–T* path.

REACTION HISTORY

The textural and compositional features of the rocks suggest first, that 'peak garnet' compositions formed in pre-D2 time through enhanced volume diffusion within garnet at peak temperatures of *c.* 750 °C within the kyanite stability field (11–12 kbar), and second that during syn- to post-D2 time reactions involving the dissolution of garnet and the formation of Al-silicate were triggered upon decompression and cooling, from the kyanite, to the sillimanite, and to the andalusite stability fields. In this section we discuss this reaction history, the main focus being to test whether the *P–T* path inferred from textural relations and thermobarometry is consistent with theoretical expectations. The discussion is done within the framework of the qualitative *P–T* grid (K_2O-Na_2O-FeO-MgO-Al_2O_3-SiO_2-H_2O, or KNFMASH, system) of Fig. 9.

Reference grid

The construction of the grid follows the phase relations devised by Thompson (1982) for the KFASH system, expanded for the extra component Na_2O assuming the partition $X_K^{Ms} > X_K^{Kfs} > X_K^{L} > X_K^{Pl}$ ($X_K = K/(K+Na)$), that the liquid has higher H_2O contents than hydrous phases muscovite and biotite, and that $Mg\#^{Grt} < Mg\#^{L} < Mg\#^{Bt}$. The latter assumption, instead of $Mg\#^{L} < Mg\#^{Grt} < Mg\#^{Bt}$ as favoured by Thompson (1982; see also Abbott & Clarke, 1979; and Abbott, 1985), is based on a number of experiments and arguments by Green (1976), Clemens & Wall (1981), Grant (1985), Le Breton & Thompson (1988), Vielzeuf & Holloway (1988) and Patiño Douce (1996) for both fluid-present and fluid-absent melting of pelite in the range 750–900 °C. However, it should be noted that Patiño Douce (1996) has suggested that the Fe-Mg partitioning between biotite and melt experiences a reversal at *c.* 750 °C (at 10 kbar), causing the melt to have $Mg\#^{Grt} < Mg\#^{Bt} < Mg\#^{L}$ at low temperature, similar to the reversal that the Fe-Mg partitioning between garnet and liquid experiences at temperatures in excess of 900 °C (for which $Mg\#^{melt} < Mg\#^{Grt}$; Green, 1977; Ellis, 1986; Vielzeuf & Holloway, 1988; Patiño Douce, 1996; but see Carrington & Harley, 1995; for different results). Consequently, a number of KNFMASH topological configurations and reaction stoichiometries are possible, depending on the type of partitioning. This is illustrated in Fig. 10 for the reactions that describe the hydrous melting of pelitic rocks, i.e. the KNFMASH divariant reactions (absent phases in place of equal sign):

$$Grt + Ms\ [St,\ Kfs,\ L]\ Bt + Als + Qtz + Pl + V \quad (3)$$

$$Qtz + Pl + Ms + Bt + V\ [Als,\ Kfs,\ St]\ Grt + L, \quad (4)$$

$$Qtz + Pl + Ms + Grt + V\ [Bt,\ Kfs,\ St]\ Als + L, \quad (5)$$

$$Grt + Ms + Pl + Qtz\ [V,\ St,\ Kfs]\ Als + Bt + L \quad (6)$$

$$Qtz + Pl + Bt + Als + V\ [Ms,\ St,\ Kfs]\ Grt + L, \quad (7)$$

$$Qtz + Pl + Ms + Bt + V\ [Kfs,\ St,\ Grt]\ Als + L, \quad (8)$$

and the associated univariant reaction [Kfs, St], which takes the forms:

$$Grt + Ms + Qtz + Pl + V\ [Kfs,\ St]\ Bt + Als + L \quad (9)$$

$$Grt + Bt + Ms + Qtz + Pl + V\ [Kfs,\ St]\ Als + L \quad (10)$$

$$Bt + Ms + Qtz + Pl + V\ [Kfs,\ St]\ Grt + Als + L \quad (11)$$

for (a) $Mg\#^{L} < Mg\#^{Grt} < Mg\#^{Bt}$, (b) $Mg\#^{Grt} < Mg\#^{L} < Mg\#^{Bt}$ and (c) $Mg\#^{Grt} < Mg\#^{Bt} < Mg\#^{L}$, respectively. The effect of pressure on Fe-Mg partitioning among garnet, biotite and melt, calculated for 750 °C with the partition equations of Patiño Douce (1996) is shown in Fig. 11(a). It can be seen that $Mg\#^{Grt} < Mg\#^{Bt} < Mg\#^{L}$ (case c) at high pressure, but that $Mg\#^{Grt} < Mg\#^{L} < Mg\#^{Bt}$ (case b) at pressures lower than 10 kbar. Hence, if reversals in the Fe-Mg partitioning among coexisting phase occurs, reactions (9)–(11) are not exclusive, but related by singular points along a single KNFMASH univariant equilibrium defined by reactions (11) at high-*P* (10) at intermediate-*P* and even (9) at low-*P*. For simplicity, however, we have assumed case (b) and the associated univariant KNFMASH reaction (10) in Fig. 9.

Figure 9 also shows the KNFMASH univariant reaction:

$$St + Ms + Qtz\ [Kfs,\ L]\ Grt + Als + Bt + Pl + V \quad (12)$$

that describes the upper stability limit of staurolite. This reaction is terminal (Thompson, 1976) since it is assumed that $Mg\#^{Grt} < Mg\#^{St} < Mg\#^{Bt}$, as indicated by natural assemblages in pelites of normal composition (i.e. with low to intermediate Mg#; e.g. Spear & Cheney, 1989; García-Casco & Torres-Roldán, 1996). Note that in the more complex KNCFMASH system, plagioclase and garnet bear Ca-components and plagioclase should appear in the left hand side of reaction (12) (cf. García-Casco & Torres-Roldán, 1996).

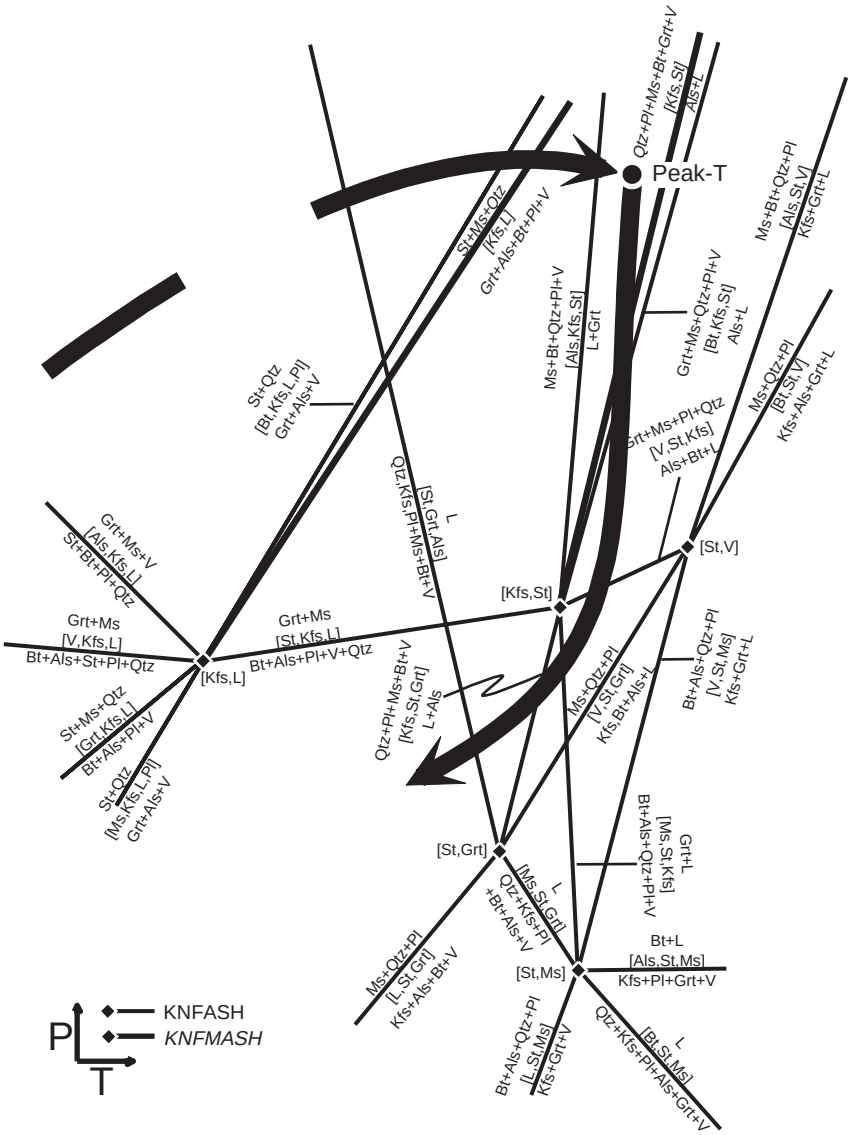

Fig. 9. Arrangement of phase relations among Kfs, Pl, Ms, Bt, St, Grt, Als, Qtz, H_2O (V), and silicate liquid (L) in the KNFASH and KNFMASH systems. Cordierite, that stabilizes at low-*P* making metastable some of the equilibria, has been omitted because it was not observed in the studied rocks, nor has it been described previously in the Pinos terrane. Dashed and solid arrows represent a hypothetical prograde *P–T* path and the proposed retrograde decompression + cooling *P–T* path of the studied rocks, respectively.

Prograde path

In the high-grade rocks direct evidence about the evolution from medium to high grade conditions along the prograde path (e.g. relict inclusions) is lacking. However, the pelitic gneisses have bulk compositions comparable to those of the medium grade metapelites of the Pinos terrane, which contain pre-D2 staurolite and kyanite. This makes it conceivable that the pelitic gneisses had followed a prograde *P–T* path at high pressure (pre-D2), along which they should have intersected univariant reaction 12 [Kfs, L] and/or the associated divariant reactions (Fig. 9) that consume staurolite and produce garnet, biotite, and kyanite, in accordance with the observed pre-D2 assemblages. The estimated peak conditions reached at the end of this prograde path (*c.* 750 and 11–12 kbar) appear to be sufficient for wet-melting of metapelite, although not for H_2O-fluid absent melting of metapelite (Fig. 8b; Patiño Douce & Harris, 1998; see also Spear *et al.*, 1999). Wet melting of metapelite produces trondhjemitic melts, as observed in the Pinos terrane,

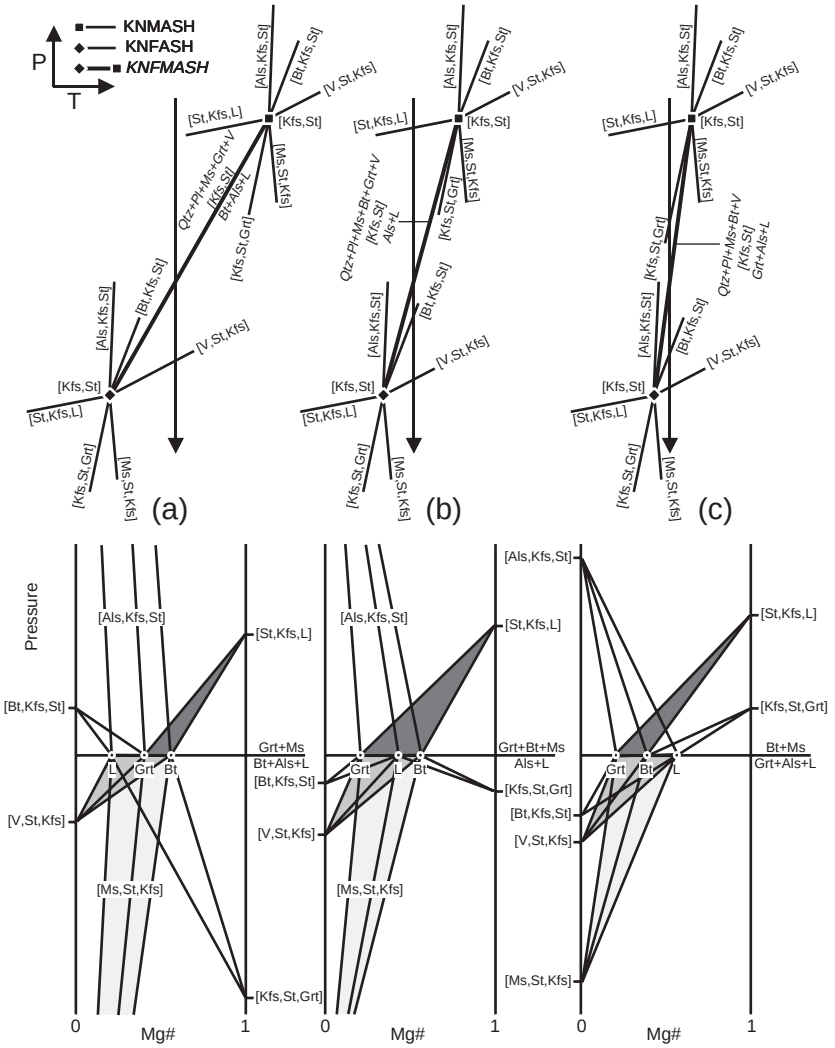

Fig. 10. *P–T* and associated isobaric *P*-Mg# diagrams (KNFMASH system) showing the arrangement of univariant reactions (9)–(11) and divariant reactions (3)–(8) for cases (a) $Mg\#^{L} < Mg\#^{Grt} < Mg\#^{Bt}$, (b) $Mg\#^{Grt} < Mg\#^{L} < Mg\#^{Bt}$, and (c) $Mg\#^{Grt} < Mg\#^{Bt} < Mg\#^{L}$ discussed in the text. In all cases, invariant point [Kfs, St] plots at higher pressure and temperature in the bounding KNMASH system, as indicated by experiments and thermodynamic properties of the solids (e.g. Thompson, 1982; Vielzeuf & Holloway, 1988). The divariant reactions intersected upon decompression (denoted by the shaded loops) drive the coexisting phases towards Fe-richer compositions. For simplicity, the loops are represented by straight lines rather than curves.

while H_2O-fluid absent melting produces granitic melts (Fig. 2b; Patiño Douce & Harris, 1998).

Melting during decompression

Wet melting at high pressure should progress through the univariant reaction (11) and/or the associated divariant reactions (case c of Fig. 10). However, the Fe-Mg partitioning in the Pinos terrane is $Mg\#^{Grt} < Mg\#^{IJ11} < Mg\#^{Bt}$ (Fig. 11b), which implies reaction (10) (case b of Fig. 10) as predicted for intermediate *P*. This suggests that wet melting was either triggered or enhanced during decompression of the terrane, consistent with existing textural evidence indicating that the trondhjemitic material segregated during D2. Further, the critical requirement of availability of H_2O-fluid is documented in the lower grade rocks by abundant fluid inclusions, fluid-assisted compositional modification of garnet along fractures and other reaction textures related to syn-D2 decompression (unpublished data). Progress of reactions (3) [St, Kfs, L] (10) [St, Kfs] (6) [V, St, Kfs] and/or (7) [Ms, St, Kfs] upon decompression, as predicted by the topological arrangement of Fig. 10(b), can adequately describe the formation of kyanite and fibrolite after garnet dissolution, and the drift of garnet and biotite composition towards Fe-richer compositions.

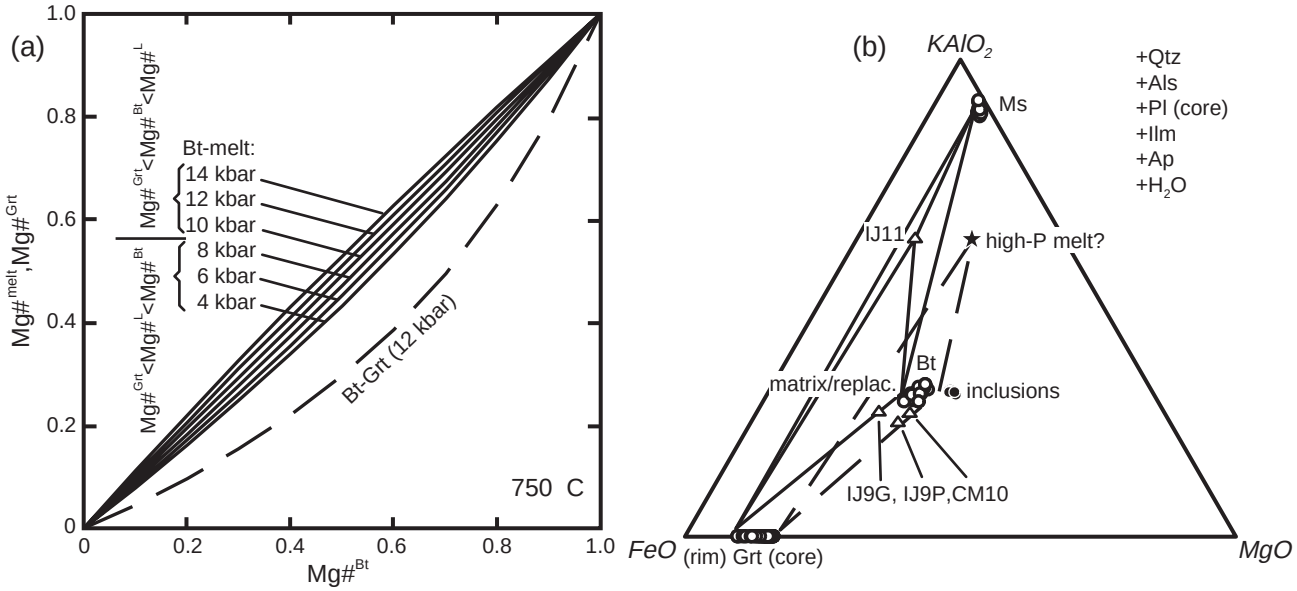

Fig. 11. (a) Reversal of Fe–Mg partitioning between biotite and melt as a function of pressure calculated using the equations given by Patiño Douce (1996) at 750 °C. The Fe–Mg partitioning between biotite and garnet does not change significantly upon changes in pressure (the curve for 12 kbar is shown for reference). (b) Phase relationships for pelitic gneiss IJ9 projected from Qtz + Als + Pl(core) + Ilm + Ap + H_2O onto the $KAlO_2$–FeO–MgO (KFM) plane, where $Mg\#^{Grt} < Mg\#^{IJ11} < Mg\#^{Bt}$ as in case (b) of Fig. 10. This phase diagram (and the AFM diagram of Fig. 8a) includes H_2O as a projection point since we infer fluid infiltration during partial melting.

Crystallization of trondhjemitic partial melts and subsolidus cooling

Cooling of trondhjemitic melts at pressures above the invariant point [St, Grt] (i.e. >4–5 kbar, Thompson, 1982; Spear *et al*., 1999) can produce muscovite with or without minor amounts of K-feldspar according to reaction [St, Grt, Als] (Fig. 9), as observed. On the other hand, further cooling and decompression under subsolidus conditions (i.e. *c.* 3 kbar, <600 °C) is consistent with the Bt + Pl + And replacements after Ms + Grt being formed through reaction (3) [St, Kfs, L] within the andalusite stability field. That reacting muscovite did not produce Kfs + Als is also an indication that the reaction:

$$Ms + Qtz + Pl\ [L, St, Grt]\ Kfs + Als + Bt + V \quad (13)$$

(Fig. 9) was not intersected at this stage, suggesting that substantial cooling accompanied retrograde evolution after the decompression stage.

TECTONIC IMPLICATIONS

The data and interpretation of reaction textures and thermobarometric calculations indicate the high grade rocks in the Pinos terrane reached peak temperature within the kyanite stability field (*c.* 750 °C and 11–12 kbar) and that the growth of fibrolite took place upon decompression and deformation (D2) in the presence of partial melts of trondhjemitic composition formed upon wet melting of metapelites.

Decompression and cooling from the kyanite to the andalusite stability fields, and thermochronological indications of fast cooling at low pressure, suggest a continuous retrograde *P*–*T* path where decompression dominated at high to intermediate pressure (steeper

Table 2. Representative analyses of garnet, mica, and feldspar from high grade rocks of the Pinos terrane.

	Garnet					
Sample	IJ9	IJ9	inc. Ky	matrix	IP5	IP5
Comment	core	rim	CM10	(core)/(rim)	core	rim
SiO_2	36.99	37.27	37.72	37.35	36.76	36.49
Al_2O_3	21.20	21.33	21.74	21.28	21.17	20.90
FeO	35.17	34.22	34.36	35.19	34.75	33.18
MnO	1.64	4.40	1.78	3.78	1.60	5.17
MgO	3.48	2.05	3.52	2.33	3.54	2.05
CaO	1.62	1.34	1.65	1.46	1.98	1.72
Total	100.10	100.61	100.77	101.39	99.80	99.51
Cations per 12 oxygen						
Si	2.98	3.00	3.00	2.99	2.96	2.98
Al	2.01	2.02	2.04	2.01	2.01	2.01
Fe	2.37	2.30	2.28	2.35	2.34	2.27
Mn	0.11	0.30	0.12	0.26	0.11	0.36
Mg	0.42	0.25	0.42	0.28	0.43	0.25
Ca	0.14	0.12	0.14	0.13	0.17	0.15
Mg#	0.15	0.10	0.15	0.11	0.15	0.10
Alm	0.78	0.78	0.77	0.78	0.77	0.75
Sps	0.04	0.10	0.04	0.09	0.04	0.12
Prp	0.14	0.08	0.14	0.09	0.14	0.08
Grs	0.05	0.04	0.05	0.04	0.06	0.05

Table 2. Continued

	Biotite									Muscovite			
Sample Comm.	IJ9 inc Grt	IJ9 after Grt	IJ9 after Grt	CM10 inc Grt	CM10 matrix	IP5 inc Grt	IP5 matrix	IJ11 inc Pl	IJ11 matrix	IJ9 matrix	IJ11 matrix high Ti	IJ11 matrix low Ti	IJ17 pegm
SiO_2	35.32	34.52	33.49	35.51	35.02	35.53	34.99	34.28	34.36	46.69	46.13	46.61	47.11
TiO_2	2.39	3.69	1.75	2.67	2.66	2.33	2.83	3.73	3.34	1.21	1.71	0.28	0.08
Al_2O_3	20.47	19.78	19.81	19.91	19.66	20.52	19.20	18.95	19.29	34.82	34.91	36.19	35.48
FeO	18.66	20.98	23.48	18.50	20.98	17.28	20.90	21.68	21.87	1.34	1.16	1.19	1.24
MnO	0.05	0.12	0.09	0.01	0.06	0.07	0.15	0.22	0.25	0.03	0.01	0.00	0.01
MgO	8.90	6.84	6.94	9.50	7.93	9.57	7.55	6.61	6.59	0.93	0.78	0.69	0.98
Na_2O	0.34	0.27	0.19	0.42	0.25	0.21	0.18	0.14	0.12	0.70	0.54	0.36	0.71
K_2O	8.92	9.20	8.81	8.48	8.73	8.78	8.70	8.96	9.05	10.33	10.30	10.39	10.40
Sum	95.05	95.40	94.56	95.00	95.29	94.29	94.50	94.57	94.87	96.05	95.54	95.71	96.01
Cations per 22 oxygen													
Si	5.34	5.29	5.24	5.36	5.35	5.38	5.39	5.32	5.32	6.17	6.12	6.15	6.21
Ti	0.27	0.43	0.21	0.30	0.31	0.27	0.33	0.44	0.39	0.12	0.17	0.03	0.01
Al	3.65	3.57	3.65	3.54	3.54	3.66	3.49	3.47	3.52	5.42	5.46	5.63	5.51
Fe^{2+}	2.36	2.69	3.07	2.34	2.68	2.19	2.69	2.81	2.83	0.15	0.13	0.13	0.14
Mn	0.01	0.02	0.01	0.00	0.01	0.01	0.02	0.03	0.03	0.00	0.00	0.00	0.00
Mg	2.01	1.56	1.62	2.14	1.81	2.16	1.73	1.53	1.52	0.18	0.15	0.14	0.19
Na	0.10	0.08	0.06	0.12	0.07	0.06	0.05	0.04	0.04	0.18	0.14	0.09	0.18
K	1.72	1.80	1.76	1.63	1.70	1.69	1.71	1.77	1.79	1.74	1.74	1.75	1.75
Mg#	0.46	0.37	0.35	0.48	0.40	0.50	0.39	0.35	0.35	0.55	0.55	0.51	0.58

Table 2. Continued

	Plagioclase									K-feldspar	
Sample Comm.	IJ9 core	IJ9 after Grt + Ms	CM10 core	CM10 after Grt	IP5 core	IJ11 core	IJ11 matrix	IJ17 after MS	IJ17 matrix	IJ11 matrix	IJ17 after MS
SiO_2	62.81	61.85	63.18	62.12	61.31	61.53	64.97	67.76	64.72	65.51	64.81
Al_2O_3	22.61	24.21	23.54	24.20	25.24	25.15	21.77	20.18	21.80	18.89	18.35
CaO	3.78	5.38	4.83	5.57	6.45	6.17	2.48	0.87	2.67	0.00	0.01
Na_2O	9.50	8.58	8.98	8.40	7.98	8.71	10.26	11.22	10.05	0.50	1.06
K_2O	0.34	0.25	0.10	0.11	0.28	0.20	0.20	0.21	0.33	15.67	15.41
Sum	99.04	100.27	100.63	100.40	101.26	101.76	99.68	100.24	99.57	100.57	99.64
Cations per 8 oxygens											
Si	2.81	2.74	2.78	2.74	2.69	2.69	2.87	2.96	2.86	2.99	3.00
Al	1.19	1.26	1.22	1.26	1.31	1.30	1.13	1.04	1.14	1.02	1.00
Ca	0.18	0.26	0.23	0.26	0.30	0.29	0.12	0.04	0.13	0.00	0.00
Na	0.82	0.74	0.77	0.72	0.68	0.74	0.88	0.95	0.86	0.04	0.10
K	0.02	0.01	0.01	0.01	0.02	0.01	0.01	0.01	0.02	0.91	0.91
An	0.18	0.25	0.23	0.27	0.30	0.28	0.12	0.04	0.13	0.00	0.00
Ab	0.80	0.73	0.77	0.73	0.68	0.71	0.87	0.95	0.86	0.05	0.10
Or	0.02	0.01	0.01	0.01	0.02	0.01	0.01	0.01	0.02	0.95	0.91

dP/dT slope), while cooling was progressively more important at low pressure (low dP/dT slope) until metamorphism terminated during the Uppermost Cretaceous (68 ± 2 Ma at *c.* 400 °C). This type of P–T path is typical of metamorphic regions affected by fast decompression, which in turn indicates either fast erosion or tectonic extension (Albaréde, 1976; Draper & Bone, 1981; Thompson & Ridley, 1987; Ridley, 1989; Monié *et al.*, 1994; Platt *et al.*, 1998; Ring *et al.*, 1999). The intimate relation between D2 and decompression (plus minor cooling) is better explained by tectonic extension, in agreement with the recent suggestion by Draper (2001) of core-complex formation in the Pinos and other south-western Cuban terranes. However, it is also remarkable that the proposed extensional event in the Pinos terrane overlaps in time with the 75–60 Ma onset of opening of the adjacent Yucatan basin (Rosencrantz, 1990, 1996), which may suggest that these two events were related.

Pre-D2 high temperatures at high pressure in the highest grade rocks confirms that metamorphism in the Pinos terrane originated within a tectonic setting of collision and crustal thickening, at variance with other south-western Cuban terranes that are characterized by high-P subduction-related metamorphism. However, age relationships do suggest that crustal thickening originated with the Upper Cretaceous collision of the Yucatan-North American margin with the Great

Volcanic Arc of the Caribbean (Pindell & Barrett, 1990; Iturralde-Vinent, 1996; Millán, 1997b).

ACKNOWLEDGEMENTS

We thank J. T. Cordova and the staff of the Empresa Geólogo-Minera Isla de la Juventud for providing the well-core samples used in this study and for their help during field work in the Pinos Island. Constructive criticism and comments by M. Brown, A. Patiño Douce, D. Whitney and an anonymous reviewer are acknowledged. This paper is part of the IGCP project 433 (Caribbean Plate Tectonics) and has received financial support from the Spanish DGES-MEC (Project PB96-1426) and the Cuban MINBAS.

REFERENCES

Abbott, R. N., 1985. Muscovite-bearing granites in the AFM liquidus projection. *Canadian Mineralogist*, **23,** 553–561.

Abbott, R. N. & Clarke, D. B., 1979. Hypothetical liquidus relationships in the subsystem Al_2O_3-FeO-MgO projected from quartz, alkali feldspar and plagioclase for a $(H_2O) \leq 1$. *Canadian Mineralogist*, **17,** 549–560.

Albaréde, F., 1976. Thermal models of post-tectonic decompression as exemplified by the Haut-Allier granulites (Massif Central, France). *Bulletin de la Société Géologique de France*, **7,** 1023–1032.

Ashworth, J. R., 1985. Introduction. In: *Migmatites* (ed. Ashworth, J. R.), pp. 1–35. Blackie and Sons Ltd, Glasgow.

Babushkin, V. & others, 1990. Informe de los trabajos de levantamiento geológico-geofísicos a escala 1: 50 000 y búsquedas acompañantes en el municipio especial Isla de la Juventud en colaboración con la URSS. Oficina Nacional de Recursos Minerales. MINBAS. La Habana, Cuba (unpublished report).

Barker, F., 1979. Trondhjemites: Definition, environment and hypotheses of origin. In: *Trondhjemites, Dacites and Related Rocks* (ed. Barker, F.). Elsevier, Amsterdam, 1–12.

Berman, R. G., 1988. Internally-consistent thermodynamic data for minerals in the system Na_2O-K_2O-CaO-MgO-FeO-Fe_2O_3-Al_2O_3-SiO_2-TiO_2-H_2O-CO_2. *Journal of Petrology*, **29,** 445–452.

Berman, R. G., 1991. Thermobarometry using multi-equilibrium calculations: a new technique, with petrological applications. *Canadian Mineralogist*, **29,** 833–855.

Berman, R. G., Aranovich, L. & Ya., 1996. Optimized standard state and mixing properties of minerals. I. Model calibration of olivine, orthopyroxene, cordierite, garnet, and ilmenite in the system FeO-MgO-CaO-Al_2O_3-TiO_2-SiO_2. *Contributions to Mineralogy and Petrology*, **126,** 1–24.

Brown, M. & Earle, M. M., 1983. Cordierite-bearing schists and gneisses from Timor, eastern Indonesia: *P–T* conditions of metamorphism and tectonic implications. *Journal of Metamorphic Geology*, **1,** 183–203.

Buguelski, Y., Vázquez, O. & Grigorieva, I., 1985. *Ore Deposits of Cuba* (in Russian), Nauka, Moscow.

Burke, K., 1988. Tectonic evolution of the Caribbean. *Annual Reviews of Earth and Planetary Science*, **16,** 201–230.

Carrington, D. P. & Harley, S. L., 1995. Partial melting and phase relations in high-grade metapelites: an experimental petrogenetic grid in the KFMASH system. *Contributions to Mineralogy and Petrology*, **120,** 270–291.

Chakraborty, S. & Ganguly, J., 1991. Compositional zoning and cation diffusion in garnets. In: *Diffusion, Atomic Ordering and Mass Transport* (ed. Ganguly, J.), *Advances in Physical Geochemistry*, 8. Springer-Verlag, New York, 120–175.

Chatterjee, N. D. & Froese, E., 1975. A thermodynamic study of the pseudobinary join muscovite-paragonite in the system $KAlSi_3O_8$-$NaAlSi_3O_8$-Al_2O_3-SiO_2-H_2O. *American Mineralogist*, **60,** 985–993.

Clemens, J. D. & Wall, V. J., 1981. Origin and crystallization of some peraluminous (S-type) granitic magmas. *Canadian Mineralogist*, **19,** 111–131.

Cobiella-Reguera, J. L., 2000. Jurassic and Cretaceous Geological History of Cuba. *International Geology Review*, **42,** 594–616.

Draper, G., 2001. *The Southern Metamorphic Terranes of Cuba as Metamorphic Core Complexes Exhumed by Low-Angle Extensional Faulting?* Transactions of the IV Congreso de Geología Y Minería, GEOMIN 2001, la Habana (edited in, C.D.-rom).

Draper, G. & Barros, J. A., 1994. Cuba. In: *Caribbean Geology: an Introduction* (eds Donovan, S. K. & Jackson, T. A.) pp. 65–86. U. W. I. Publishers' Association, Kingston, Jamaica.

Draper, G. & Bone, R., 1981. Denudation rates, thermal evolution, and preservation of blueschists terrains. *Journal of Geology*, **89,** 601–613.

Draper, G., Jackson, T. A. & Donovan, S. K., 1994. Geologic provinces of the Caribbean Region. In: *Caribbean Geology: an Introduction* (eds Donovan, S. K. & Jackson, T. A.) pp. 3–12. U. W. I. Publishers' Association, Kingston, Jamaica.

Ellis, D. J., 1986. Garnet-liquid Fe^{2+}-Mg equilibria and implications for the beginning of melting in the crust and subduction zones. *American Journal of Science*, **286,** 765–791.

Fuhrman, M. L. & Lindsley, D. H., 1988. Ternary-feldspar modeling and thermometry. *American Mineralogist*, **73,** 201–215.

García-Casco, A., Sánchez-Navas, A. & Torres-Roldán, R. L., 1993. Disequilibrium decomposition and breakdown of muscovite in high *P–T* gneisses, Betic alpine belt (southern Spain). *American Mineralogist*, **78,** 158–177.

García-Casco, A. & Torres-Roldán, R. L., 1996. Disequilibrium induced by fast decompression in St-Bt-Grt-Ky-Sil-And metapelites from the Betic Belt (Southern Spain). *Journal of Petrology*, **37,** 1207–1239.

Goncalves, P., Guillot, S., Lardeaux, J.-M., Nicollet, C. & de Mercier Lepinay, B., 2000. Thrusting and sinistral wrenching in a pre-Eocene HP-LT Caribbean accretionary wedge (Samaná Peninsula, Dominican Republic). *Geodinamica Acta*, **13,** 119–132.

Gordon, M. B., Mann, P., Cáceres, D. & Flores, R., 1997. Cenozoic tectonic history of the North America–Caribbean plate boundary in western Cuba. *Journal of Geophysical Research*, **102,** 10 055–10 082.

Grant, J. A., 1985. Phase equilibria in partial melting of pelitic rocks. In: *Migmatites* (ed. Ashworth, J. R.), pp. 86–144. Blackie and Sons Ltd, Glasgow.

Green, T. H., 1976. Experimental generation of cordierite- or garnet-bearing granitic liquids from a pelitic composition. *Geology*, **4,** 85–88.

Green, T. H., 1977. Garnet in silicic liquids and its possible use as a *P–T* indicator. *Contributions to Mineralogy and Petrology*, **65,** 59–67.

Guidotti, C. V., 1984. Micas in metamorphic rocks. In: *Micas* (ed. Bailey, S. W.), pp. 357–468. Reviews in Mineralogy, 13, Mineralogical Society of America, Washington DC.

Iturralde-Vinent, M. A., 1996. Introduction to Cuban Geology and Geophysics. In: *Ofiolitas Y Arcos Volcánicos de Cuba* (ed. Iturralde-Vinent, M. A.), pp. 3–35. IGCP Project 364 Special Contribution, 1, IGCP, Miami.

Iturralde-Vinent, M. A., 1997. Introducción a la Geología de Cuba. In: *Estudios Sobre Geología de Cuba* (eds Furrazola Bermúdez, G. F. & Núñez Cambra, K. E.), pp. 35–68. Centro Nacional de Información Geológica, La Habana, Cuba.

Iturralde-Vinent, M. A., Millán, G., Korkas, L., Nagy, E. & Pajón, J., 1996. Geological interpretation of the Cuban K-Ar

data base. In: *Ofiolitas Y Arcos Volcánicos de Cuba* (ed. Iturralde-Vinent, M. A.), pp. 48–69. IGCP Project 364 Special Contribution, 1, IGCP, Miami.

Joyce, J., 1991. Blueschist metamorphism and deformation on the Samana Peninsula; A record of subduction and collision in the Greater Antilles. In: *Geologic and Tectonic Development of the North America–Caribbean Plate Boundary in Hispaniola* (eds Mann, P., Draper, G. & Lewis, J. F.), pp. 47–76. Geological Society of America Special Paper, 262, Geological Society of America, Boulder.

Kohn, M. J. & Spear, F. S., 2000. Retrograde net transfer reaction insurance for pressure-temperature estimates. *Geology*, **28** (12), 1127–1130.

Kretz, R., 1983. Symbols for rock-forming minerals. *American Mineralogist*, **68,** 277–279.

Le Breton, N. & Thompson, A. B., 1988. Fluid-absent (dehydration) melting of biotite in metapelites in the early stages of crustal anatexis. *Contributions to Mineralogy and Petrology*, **99,** 226–237.

Lewis, J. F. & Draper, G., 1990. Geology and tectonic evolution of the northern Caribbean margin. In*: The Geology of North America, the Caribbean Region* (eds Dengo, G. & Case, J. E.), pp. 77–140, Geological Society of America, Boulder.

Mann, P., 1999. Caribbean sedimentary basins: Classification and tectonic setting. In: *Caribbean Basins* (ed. Mann, P.), pp. 3–31, Sedimentary Basins of the World, 4. Elsevier Science, Amsterdam.

Marton, G. L. & Buffler, R. T., 1999. Jurassic-Early Cretaceous tectono-paleogeographic evolution of the Southeastern Gulf of Mexico basin. In: *Caribbean Basins* (ed. Mann, P.), pp. 63–91, *Sedimentary Basins of the World*, 4. Elsevier Science, Amsterdam.

McDonough, W. F. & Sun, S.-S., 1995. The composition of the Earth. *Chemical Geology*, **120,** 223–253.

Millán, G., 1981. Geología del macizo metamórfico de la Isla de la Juventud. *Ciencias de la Tierra Y Del Espacio*, **3,** 3–22.

Millán, G., 1988. La asociación glaucofana-pumpellita en metagrabroides de la faja metamórfica Cangre. *Boletín de Geociencias*, **3** (2)**,** 35–36.

Millán, G., 1997a. Posición estratigráfica de las metamorfitas cubanas. In: *Estudios Sobre Geología de Cuba* (eds Furrazola Bermúdez, G. F. & Núñez Cambra, K. E.). Centro Nacional de Información Geológica, La Habana, Cuba, 251–258.

Millán, G., 1997b. Geología del macizo metamórfico de la Isla de la Juventud. In: *Estudios Sobre Geología de Cuba* (eds Furrazola Bermúdez, G. F. & Núñez Cambra, K. E.). Centro Nacional de Información Geológica, La Habana, Cuba, 259–270.

Millán, G., 1997c. Geología del macizo metamórfico del Escambray. In: *Estudios Sobre Geología de Cuba* (eds Furrazola Bermúdez, G. F. & Núñez Cambra, K. E.), pp. 271–288, Centro Nacional de Información Geológica, La Habana, Cuba.

Millán, G. & Somin, M. L., 1981. *Litología, Estratigrafía, Tectónica Y Metamorfismo Del Macizo Del Escambray*. Editora ACC, La Habana.

Millán, G. & Somin, M. L., 1985. Contribución al conocimiento geológico de las metamorfitas del Escambray y Purial. *Reporte de Investigación, 2.* Academia de Ciencias de Cuba, La Habana.

Miller, C. F., Stoddard, E. F., Bradfish, L. J. & Dollase, W. A., 1981. Composition of plutonic muscovite: genetic implications. *Canadian Mineralogist*, **19,** 25–34.

Monié, P., Torres-Roldán, R. L. & García-Casco, A., 1994. Cooling and exhumation of the western Betic Cordilleras, $^{40}Ar^{39}Ar$ thermochronological constraints on a collapsed terrane. *Tectonophysics*, **238,** 353–379.

O'Connor, J. T., 1965. A classification of quartz-rich igneous rocks based on feldspar ratios. *U.S. Geological Survey Professional Paper*, **525B,** B79–B84.

Pardo, M., 1990. La constitución geológica del macizo de la Isla de la Juventud y metalogenia endógena vinculada al magmatismo ácido. *Transactions of the 12th Caribbean Geological Conference, St-Croix U. S. Virgin Islands.* Miami Geological Society, Miami.

Pardo, M. & De Moya, I., 1988. Nuevos datos sobre la estructura geológica de la Isla de la Juventud. Parte II: Estructura interna del macizo metamórfico. *Revista Tecnológica*, **18** (3)**,** 3–12.

Patiño Douce, A. E., 1996. Effects of pressure and H_2O content on the composition of primary crustal melts. *Transactions of the Royal Society of Edinburgh, Earth Sciences*, **87,** 11–21.

Patiño Douce, A. E. & Harris, N., 1998. Experimental constraints on Himalayan anatexis. *Journal of Petrology*, **39,** 689–710.

Pattison, D. R. M., 1992. Stability of andalusite and sillimanite and the Al_2SiO_5 triple point: constraints from de Ballachulish aureole, Scotland. *Journal of Geology*, **100,** 423–446.

Pindell, J. L. & Barrett, S. F., 1990. Geologic evolution of the Caribbean region; A plate-tectonic perspective. In: *The Caribbean Region, The Geology of North America* (eds Dengo, G. & Case, J. E.), pp. 405–432, Geological Society of America, Boulder.

Platt, J. P., Soto, J. I., Whitehouse, M. J., Hurford, A. J. & Kelley, S. P., 1998. Thermal evolution, rate of exhumation, and tectonic significance of metamorphic rocks from the floor of the Alboran extensional basin, western Mediterranean. *Tectonics*, **17,** 671–689.

Pszczólkowski, A., 1987. Paleogeography and paleotectonic evolution of Cuba and adjoining areas during the Jurassic-Early Cretaceous. *Annales de la Societé Géologique de Pologne*, **57,** 127–142.

Pszczólkowski, A., 1999. The exposed passive margin of North America in Western Cuba. In: *Caribbean Basins, Sedimentary Basins of the World*, **4** (ed. Mann, P.), pp. 93–121, Elsevier Science, Amsterdam.

Pszczólkowski, A. & de Albear, J. F., 1985. Sobre la edad del metamorfismo y la estructura tectónica de la faja Cangre, Provincia de Pinar del Río, Cuba. *Ciencias de la Tierra Y Del Espacio*, **10,** 31–36.

Ridley, J., 1989. Vertical movement in orogenic belts and the timing of metamorphism relative to deformation. In: *Evolution of Metamorphic Belts, Geological Society Special Publication*, **43** (eds Daly, J. S., Cliff, R. A. & Yardley, B. W. D.), pp. 103–115, Geological Society, London.

Ring, U., Brandon, M. T., Willett, S. D. & Lister, G. S., 1999. Exhumation processes. In: *Exhumation Processes: Normal Faulting, Ductile Flow and Erosion, Geological Society, London. Special Publications*, **154** (eds Ring, U., Brandon, M. T., Lister, G. S. & Willett, S. D.) 1–27, Geological Society, London.

Rosencrantz, E., 1990. Structure and tectonics in the Yucatan basin, Caribbean Sea, as determined from seismic reflection studies. *Tectonics*, **9,** 1037–1059.

Rosencrantz, E., 1996. Basement structure and tectonics in the Yucatan basin. In: *Ofiolitas Y Arcos Volcánicos de Cuba* (ed. Iturralde-Vinent, M. A.), pp. 36–47. IGCP Project 364, Special Contribution, 1, Miami.

Sawyer, E. W. & Barnes, S.-J., 1988. Temporal and compositional differences between subsolidus and anatectic migmatite leucosomes from the Quetico metasedimentary belt, Canada. *Journal of Metamorphic Geology*, **6,** 437–540.

Schwandt, C. S., Cygan, R. T. & Westrich, H. R., 1996. Ca self-diffusion in grossular garnet. *American Mineralogist*, **81,** 448–451.

Seck, H. A., 1971. Koexistierende Alkalifeldspäte und Plagioklase im System $NaAlSi_3O_8$-$KAlSi_3O_8$-$CaAl_2Si_2O_8$-H_2O bei temperaturen von 650 °C bis 900 °C. *Neues Jahrbuch für Mineralogie Abhandlungen*, **115,** 315–345.

Somin, M. L. & Millán, G., 1981. *Geology of the Metamorphic Complexes of Cuba* (in russian), Nauka, Moscow.

Spear, F. S., 1991. On the interpretation of peak metamorphic temperatures in light of garnet diffusion during cooling. *Journal of Metamorphic Geology*, **9,** 379–388.

Spear, F. S. & Cheney, J. T., 1989. A petrogenetic grid for pelitic schists in the system SiO_2-Al_2O_3-FeO-MgO-K_2O-H_2O. *Contributions to Mineralogy and Petrology*, **101,** 149–164.

Spear, F. S. & Florence, F. P., 1992. Thermobarometry in granulites: Pitfalls and new approaches. *Journal of Precambrian Research*, **55,** 209–241.

Spear, F. S., Kohn, M. J. & Cheney, J. T., 1999. *P–T* paths from anatectic pelites. *Contributions to Mineralogy and Petrology*, **134,** 17–32.

Spear, F. S. & Parrish, R. R., 1996. Petrology and cooling rates of the Valhalla Complex, British Columbia, Canada. *Journal of Petrology*, **37,** 733–765.

Taylor, S. R. & McLennan, S. M., 1985. *The Continental Crust: its Composition and Evolution*. Blackwell, Oxford.

Thompson, A. B., 1976. Mineral reactions in pelitic rocks: I. Prediction of *P-T*-X (Fe-Mg) phase relations. *American Journal of Science*, **276,** 401–424.

Thompson, A. B., 1982. Dehydration melting of pelitic rocks and the generation of H_2O-undersaturated granitic liquids. *American Journal of Science*, **282,** 1567–1595.

Thompson, A. B. & Ridley, J. R., 1987. Pressure-temperature-time (*P–T–t*) histories of orogenic belts. *Philosophical Transactions of the Royal Society of London*, **A321,** 27–45.

Torres-Roldán, R. L., García-Casco, A. & García-Sánchez, P. A., 2000. CSpace: An integrated workplace for the graphical and algebraic analysis of phase assemblages on 32-bit Wintel platforms. *Computers and Geosciences*, **26,** 779–793.

Tracy, R. J., 1982. Compositional zoning and inclusions in metamorphic minerals. In: *Characterization of Metamorphism Through Mineral Equilibria, Reviews in Mineralogy*, **10** (ed. Ferry, J. M.), pp. 355–397. Mineralogical Society of America, Washington D.C.

Vielzeuf, D. & Holloway, J. R., 1988. Experimental determination of the fluid-absent melting relations in the pelitic system. Consequences for crustal differentiation. *Contributions to Mineralogy and Petrology*, **98,** 257–276.

Whitney, D. L. & Irving, A. J., 1994. Origin of K-poor leucosomes in a metasedimentary migmatite complex by ultrametamorphism, synmetamorphic magmatism and subsolidus processes. *Lithos*, **32,** 173–192.

Received 22 November 2000; revision accepted 15 June 2001